Predictive Common-Mode Voltage Suppression Method Based on Current Ripple for Permanent Magnet Synchronous Motors

Xiaofan Wang, *Student member, IEEE*, Xiaochun Fang, *Member, IEEE*, Shuai Lin, Fei Lin, *Member, IEEE*, and Zhongping Yang, *Member, IEEE*

***Abstract*— Compared with the pulsewidth modulation-based field-oriented control scheme, finite control set model predictive control (FCS-MPC), which has been widely concerned, has great advantages in fast dynamic response, multiobjective control, and system constraint processing. The common-mode voltage (CMV) generated by the inverter will lead to bearing damage and electromagnetic interference issues. This paper studies CMV suppression method based on FCS-MPC for permanent magnet synchronous motor fed by voltage source inverter. The use of zero voltage vector can significantly increase the output CMV of the inverter. The method of abandoning the zero vector directly can decrease CMV, but will lead to larger current distortion. Replacing the zero vector with nonadjacent vectors is a better way but will lead to higher switching frequency. When the CMV is introduced into the cost function, the tradeoff between CMV suppression and current distortion can be realized, but there is no rule to be followed for weight coefficient design. In this paper, we propose a variable FCS scheme based on current ripple. Based on this scheme, CMV can be suppressed under the premise that the current distortion is small, and the switching frequency is not significantly increased. Based on the proposed method, current distortion and CMV can be well balanced under different load conditions by setting the relative error limits. Experimental results show that the proposed method has good control performance under various operation conditions.**

***Index Terms*— Common-mode voltage (CMV), current ripple, low switching frequency, model predictive control (MPC), permanent magnet synchronous motor (PMSM).**

I. Introduction

THANKS to the advantages of high power density, high efficiency, and high reliability, the permanent magnet synchronous motor (PMSM) drive system has been widely used in industry and transportation. The common-mode voltage (CMV) generated by power electronic inverters may cause a series of negative problems. The magnitude of the CMV amplitude is an important measure of the strength of electromagnetic interference. Large CMV can cause serious damage to the insulation between the motor windings and the motor bearings [1].

Hardware-based and software-based solutions to reduce CMV have been proposed. Compared with hardware solutions, software solutions have attracted wide attention due to their economy and flexibility. The basic idea of the pulsewidth modulation (PWM) technique is to synthesize the target voltage vector with the basic voltage vector in one control cycle. For a three-phase two-level inverter, it can output eight basic voltage vectors including two zero vectors and six nonzero vectors. The zero vector will generate a CMV of $\pm V_{dc}/2$ between the midpoint of the dc voltage and the neutral point of the motor. A nonzero vector will produce a CMV of $\pm V_{dc}/6$. Based on this idea, some CMV suppression methods are proposed, such as active zero state PWM [2]–[5], near state PWM [5], [6], and remote state PWM [7], [8]. A CMV suppression method for back-to-back current source converter is proposed in [9], which coordinates the active and zero vectors of both rectifier and inverter.

In the recent period, rapid development of modern microcontrollers has led to the development and implementation of new and more intelligent control strategies for power converters as an alternative to traditional technologies. As one of these powerful and attractive alternatives, predictive control has received special attention. Finite control set model predictive control (FCS-MPC) is an intuitive control method that does not require linear controllers and modulators, and it is easy to include nonlinear characteristics and constraints in the control laws [10]–[32]. These advantages make predictive control possible in the near future industrial applications. Based on FCS-MPC scheme, several CMV suppression methods have been studied [10]–[15]. In [10], a generalized approach based on model predictive strategy for the current control, dc-link capacitor voltages balancing, switching frequency reduction, and CMV suppression in multilevel diode clamped converters. The scheme proposed in [11] removes two zero vectors, leaving only six nonzero vectors as candidates. Mun and Kwak [12] use the idea of deadbeat control to achieve CMV suppression. Although this method can reduce the computational burden, the differential calculation will produce a lot of noise. Kwak and Mun [13] proposed to use two nonzero

Manuscript received April 19, 2018; revised October 5, 2018 and December 12, 2018; accepted January 12, 2019. Date of publication January 30, 2019; date of current version May 1, 2019. This work was supported by the Fundamental Research Funds for the Central Universities under Grant 2018YJS153. Recommended for publication by Associate Editor Margarita Norambuena. *(Corresponding author: Xiaochun Fang.)*

The authors are with the School of Electrical Engineering, Beijing Jiaotong University, Beijing 100044, China (e-mail: xfwangs@bjtu.edu.cn; xcfang@bjtu.edu.cn; 17121459@bjtu.edu.cn; flin@bjtu.edu.cn; zhpyang@bjtu.edu.cn).

Color versions of one or more of the figures in this paper are available online at http://ieeexplore.ieee.org.

Digital Object Identifier 10.1109/JESTPE.2019.2896158

voltage vectors during each sampling period so that the total harmonic distortion (THD) of the current can be reduced. However, the algorithm needs to optimize the selection of two vectors, which leads to computational complexity and high switching frequency. In [14], in order to reduce the switching frequency, switching between nonadjacent voltage vectors is prohibited, and therefore, there are only four candidate voltage vectors. (In this paper, we call this method as conventional 4VVs.) Based on the conventional 4VVs method, Guo *et al.* [15] proposed to abandon the zero vector and use a nonadjacent vector as the fourth candidate so that CMV can be well suppressed. (In this paper, we call this method as nonzero 4VVs.) However, the switching frequency of this method will be higher than conventional 4VVs.

As the core control performance indicator of motor drive system, current ripple should be given enough attention to. The main goal of this paper is to examine how it can mitigate the negative impact of CMV while keeping the current ripple within an acceptable range. Therefore, we will consider both current ripple and CMV as two key indicators in the formulation of the control law. In addition, in order to adapt this control law to different applications, we have studied how to adjust the weight of each target within a certain range.

The following sections of this paper are arranged as follows. In Section II, the basic structure of FCS-MPC for PMSM is established and the relationship between output voltage vectors of inverter and CMV is discussed. Section III shows some existing method. Section IV shows the CMV suppression method based on current ripple proposed in this paper. Section V collates and analyzes the experimental results. Section VI is the conclusion.

II. Background and Modeling

In this section, the basic content of FCS-MPC is introduced, and the FCS-MPC system of PMSM is constructed. In addition, the effect of the inverter output voltage on CMV is discussed.

A. FCS-MPC for PMSM

The model of PMSM in state-space representation is as follows:

$$\frac{d\boldsymbol{i}(t)}{dt} = \boldsymbol{F}\boldsymbol{i}(t) + \boldsymbol{G}\boldsymbol{u}(t) + \boldsymbol{E} \tag{1a}$$

where $\boldsymbol{i}(t)$ denotes stator current as the state vector, $\boldsymbol{u}(t)$ denotes the input voltage vector, with the system matrix $\boldsymbol{F}$, input matrix $\boldsymbol{G}$, and the back electromotive force $\boldsymbol{E}$, which can be described as

$$\begin{aligned} \boldsymbol{i}(t) &= [i_d(t),\ i_q(t)]^T, \quad \boldsymbol{u}(t) = [u_d(t),\ u_q(t)]^T \\ \boldsymbol{F} &= \begin{bmatrix} -R_s/L_d & L_q\omega_r\,(t)/L_d \\ -L_d\omega_r(t)/L_q & -R_s/L_q \end{bmatrix} \qquad (1b) \\ \boldsymbol{G} &= \begin{bmatrix} 1/L_d & 0 \\ 0 & 1/L_q \end{bmatrix} \\ \boldsymbol{E} &= \begin{bmatrix} 0 \\ -\psi_f\omega_r(t)/L_q \end{bmatrix} \qquad (1c) \end{aligned}$$

where i_d and i_q are the d-axis and q-axis components of the stator current, and u_d and u_q are the d-axis and q-axis components of the stator voltage. Forward Euler method can be used to translate the model from the continuous-time to the discrete-time domain:

$$\boldsymbol{i}^p(k+1) = \boldsymbol{A}\boldsymbol{i}(k) + \boldsymbol{B}\boldsymbol{u}(k) + \boldsymbol{C} \tag{2a}$$

$$\boldsymbol{i}(k) = [i_d(k), i_q(k)]^T, \boldsymbol{u}(k) = [u_d(k), u_q(k)]^T \tag{2b}$$

where $x(k)$ represents the variable x corresponding to k, $x(k+1)$ represents the variable x corresponding to $k+1$, and the superscript p represents the predicted value of the corresponding variable. The system matrix $\boldsymbol{A}$, the input matrix $\boldsymbol{B}$, and the back electromotive force $\boldsymbol{C}$ are as follows:

$$\begin{aligned} \boldsymbol{A} &= \boldsymbol{I} + \boldsymbol{F}T_s = \begin{bmatrix} 1 - R_sT_s/L_d & L_qT_s\omega_r(k)/L_d \\ -L_dT_s\omega_r(k)/L_q & 1 - R_sT_s/L_q \end{bmatrix} \\ \boldsymbol{B} &= \boldsymbol{G}T_s = \begin{bmatrix} T_s/L_d & 0 \\ 0 & T_s/L_q \end{bmatrix} \\ \boldsymbol{C} &= \boldsymbol{E}T_s = \begin{bmatrix} 0 \\ -\psi_f T_s\omega_r(k)/L_q \end{bmatrix} \end{aligned} \tag{2c}$$

where $\boldsymbol{I}$ is the identity matrix, R_s is the stator resistance, T_s is the sampling period, ω_r is the synchronous speed, L_d is the d-axis inductance, and L_q is the q-axis inductance. In order to compensate for the existence of a delay in the actual system, we need to predict the values corresponding to time step $k+2$, so (2a) is rewritten as

$$\boldsymbol{i}^p(k+2) = \boldsymbol{A}\boldsymbol{i}(k+1) + \boldsymbol{B}\boldsymbol{u}(k+1) + \boldsymbol{C}. \tag{3}$$

Due to the large mechanical inertia of the system, the approximation is considered

$$\omega_r(k+2) \approx \omega_r(k+1) \approx \omega_r(k). \tag{4}$$

Consequently, the coefficient matrices $\boldsymbol{A}$, $\boldsymbol{B}$, and $\boldsymbol{C}$ are approximated to be constants from time step k to $k+2$.

The cost function is defined according to control objects. In order to achieve current tracking control, the cost function can be defined as the distance between predictive currents and current references at time step $k+2$, which is shown in the following equation:

$$J = \left|i_{d\text{ref}} - i_d^p(k+2)\right|^2 + \left|i_{q\text{ref}} - i_q^p(k+2)\right|^2 \tag{5}$$

where $i_{d\text{ref}}$ and $i_{q\text{ref}}$ are the d-axis and q-axis current references which are considered to be constants from time step k to $k+2$.

For three-phase two-level inverters, there are eight possible switching states, corresponding to six nonzero voltage vectors and two zero voltage vectors. According to (3), each candidate voltage vector will have a corresponding value of the cost function. The smaller the cost function, the smaller the deviation between the predicted current and the reference current. Finally, the voltage vector corresponding to the minimum cost function is selected as the control command sent to the inverter.

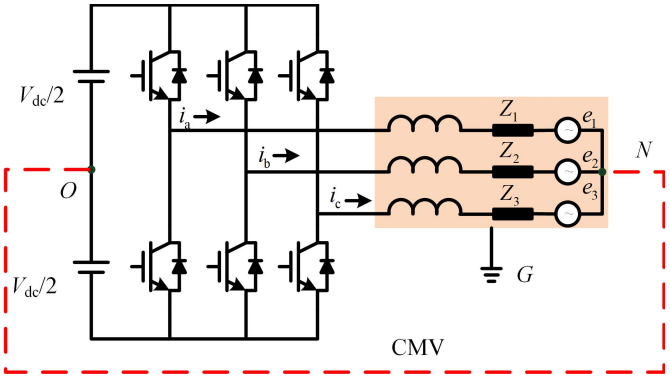

Fig. 1. Two-level three-phase inverter drive system.

TABLE I
CMV OF THREE-PHASE INVERTER

Voltage Vectors	Switch States $\{S_a,S_b,S_c\}$	Common-mode Voltage U_{NG}
v_0	{0,0,0}	$-V_{dc}/2$
v_1	{1,0,0}	$-V_{dc}/6$
v_2	{1,1,0}	$V_{dc}/6$
v_3	{0,1,0}	$-V_{dc}/6$
v_4	{0,1,1}	$V_{dc}/6$
v_5	{0,0,1}	$-V_{dc}/6$
v_6	{1,0,1}	$V_{dc}/6$
v_7	{1,1,1}	$V_{dc}/2$

B. Common-Mode Voltage Modeling

In a two-level three-phase inverter drive system, as shown in Fig. 1, the CMV is defined as U_{NG}, where $U_{NG} = U_{NO} + U_{OG}$. Since U_{OG} is negligible compared to U_{NO}, the CMV of the three-phase inverter can be expressed as

$$U_{NG} \approx U_{NO} = (U_a + U_b + U_c)/3. \tag{6}$$

Since each bridge arm has two working states, the three-phase inverter has a total of $2^3 = 8$ working states, defined as v_0, v_7. According to (6), the output CMV amplitude of the three-phase inverter can be obtained in eight operating states, as shown in Table I. The amplitude of U_{NG} has two states——$V_{dc}/6$ and $V_{dc}/2$. The CMV amplitude of the zero-vector states v_0 and v_7 is $V_{dc}/2$, and the CMV amplitude of the other vector states is $V_{dc}/6$. If the use of the zero vectors $v_0(0, 0, 0)$ and $v_7(1, 1, 1)$ is forbidden, the inverter output CMV has only the amplitude of $V_{dc}/6$, which can realize the suppression of CMV.

III. CONVENTIONAL METHOD

The candidate voltage vector selection method used in [14] is shown in Fig. 2. In this conventional 4VVs method, the number of candidate voltage vectors is reduced from 8 to 4, so the computational burden is reduced. Since switching between nonadjacent voltage vectors is forbidden, at most one bridge arm is active at each sampling period and the switching frequency of the inverter is reduced.

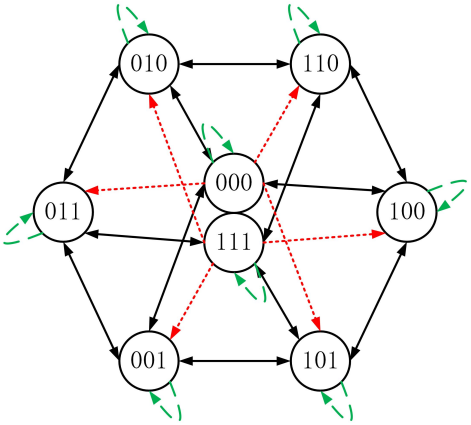

Fig. 2. Conventional 4VVs method [14].

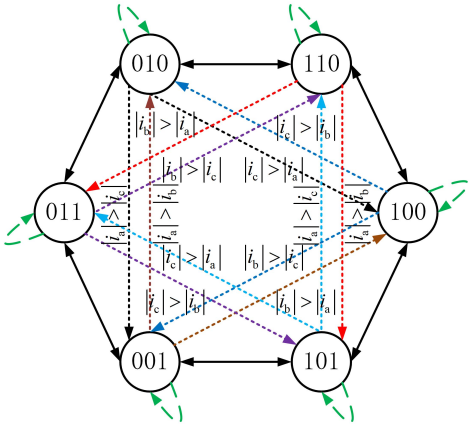

Fig. 3. Nonzero 4VVs method [15].

In order to carry out the CMV suppression, Guo *et al.* [15] use a new voltage vector selection method, as shown in Fig. 3. In this method, the use of zero vectors is forbidden, and a nonadjacent voltage vector is selected as the fourth candidate considering the instantaneous current values. In this nonzero 4VVs method, the CMV is limited to $V_{dc}/6$ and the method shows good suppression effect. However, the switching frequency of the inverter is higher than conventional 4VVs due to the use of nonadjacent vectors.

IV. PROPOSED METHOD

A. CMV Suppression Based on Variable FCS

Fig. 4 shows the algorithm of the proposed method. In order to take both current quality and CMV suppression into account, it is necessary to adjust the zero vector usage strategy in real time based on the operating state of the motor. If the use of zero vectors is completely forbidden, it will inevitably cause serious damage to the current quality, so we propose to use a variable FCS, that is, the number of candidate vectors in the FCS will be dynamically adjusted according to the predicted current error.

In order to keep the switching frequency low, we use only the adjacent voltage and zero vectors, as shown in Fig. 2, but this is not a fixed vector selection mode. The difference is

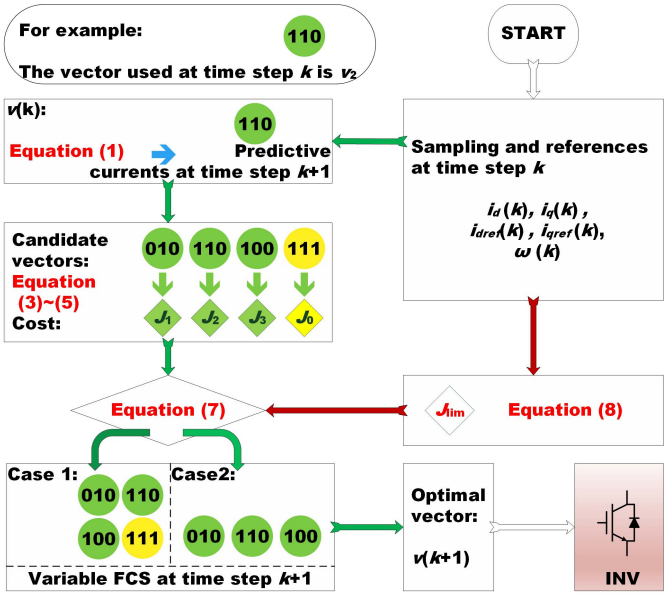

Fig. 4. Algorithm of the proposed method.

that in order to effectively suppress the CMV, we propose to prohibit the use of zero vectors in some special cases. Therefore, the key point of the proposed method is to set an evaluation criterion to dynamically change the selection mode of voltage vectors during the operation of FCS-MPC system.

In each sampling period, the candidate vector includes three nonzero vectors and one zero vector, so we can get four cost function values J_1, J_2, J_3, (calculated by nonzero vectors) and J_0 (calculated by zero vectors). Since the value of the cost function represents the deviation of the predicted current relative to the reference current, we set an error limit J_{lim}. Then, according to (7) to determine if we need to use zero vectors

$$\begin{cases} \text{case1} : \min(J_1, J_2, J_3) > J_{\text{lim}}, & J_0 = J_0 \\ \text{case2} : \min(J_1, J_2, J_3) \le J_{\text{lim}}, & J_0 \to +\infty. \end{cases} \tag{7}$$

Equation (7) contains two cases. In the first case, the cost function values for all nonzero vectors are greater than J_{lim}, which means that all of the predicted current deviations exceed the set value. In order to try to ensure better current quality, zero vector will participate in the optimization process as a normal candidate vector. In the second case, the cost function of some nonzero vectors is less than J_{lim}, which means the predicted current deviation is still less than the set value even in the absence of the zero vector. Therefore, the value of cost function of the zero vector is modified to infinity, which means that the zero vector will be removed during the optimization.

The value of the current error limit J_{lim} is determined according to the current distortion requirements, and finally the balance between the current precision control and the CMV is reached.

In many applications, the speed and load of the motor change frequently and significantly. Therefore, it is unwise to set the current error limit to a fixed value. Therefore, the value of J_{lim} can be set to vary according to current references, as is

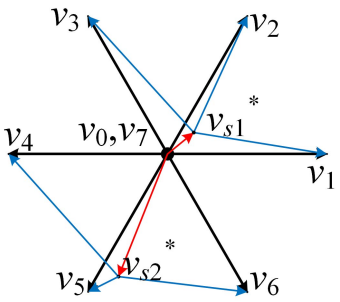

Fig. 5. Effect of ideal voltage vector.

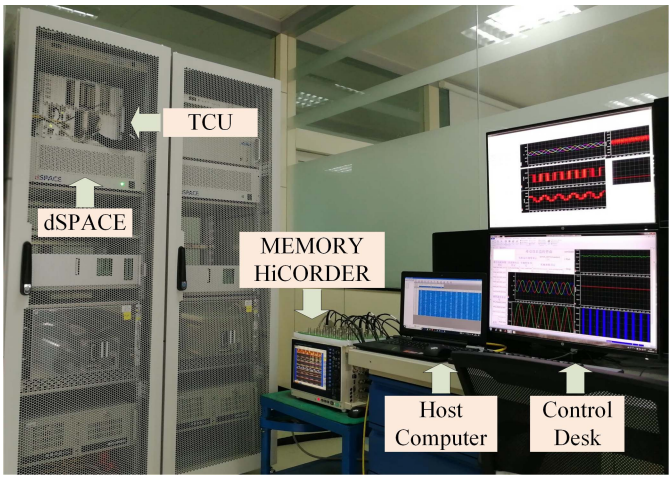

Fig. 6. Experimental platform.

shown in the following equation:

$$J_{\text{lim}} = K^2\left(i_{d\text{ref}}^2 + i_{q\text{ref}}^2\right) \tag{8}$$

where K is the current relative error limit. Obviously, larger K can lead to a stronger CMV suppression effect, while smaller K can lead to a weaker CMV suppression effect. Therefore, the balance between the current control performance and the CMV suppression can be realized by simply adjusting the parameter K, and good current quality can be obtained even at low speed or light load conditions.

B. Current Ripple Analysis

For low-switching-frequency applications, the switching ripple becomes the main component of the current distortion. In order to study the effect of CMV suppression method on current quality, the relationship between zero vector and current ripple needs to be discussed. We will derive the switching ripple current based on the mathematical model of PMSM.

According to the voltage equation of PMSM, we can get

$$\begin{cases} \dfrac{di_d}{dt} = -\dfrac{R_s}{L_d} i_d + \dfrac{\omega_r L_q}{L_d} i_q + \dfrac{u_d}{L_d} \\ \dfrac{di_q}{dt} = -\dfrac{R_s}{L_q} i_q - \dfrac{\omega_r (L_d i_d + \psi_f)}{L_q} + \dfrac{u_q}{L_q}. \end{cases} \tag{9}$$

Therefore, the amount of current change Δi_d and Δi_q in a control cycle are expressed as (10), where T_s is the

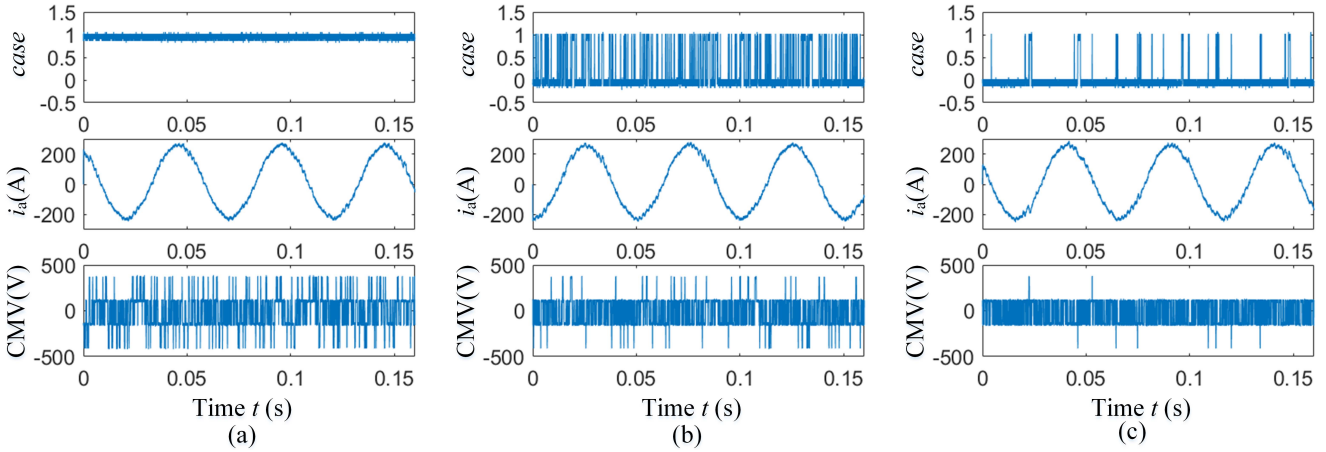

Fig. 7. Proposed method with $n = 600$ r/min, 100% load. Waveforms of case, CMV, and motor current i_a. (a) $K = 0$ and THD $= 5.57\%$. (b) $K = 0.04$ and THD $= 6.21\%$. (c) $K = 0.08$ and THD $= 6.56\%$.

sampling period

$$\begin{cases} \Delta i_d = \displaystyle\int_0^{T_s} \left(-\frac{R_s}{L_d} i_d + \frac{\omega_r L_q}{L_d} i_q + \frac{u_d}{L_d}\right) dt \\ \quad \approx \dfrac{T_s}{L_d}[u_d - (R_s i_d - \omega_r L_q i_q)] = \dfrac{T_s}{L_d}(u_d - u_d^*) \\ \Delta i_q = \displaystyle\int_0^{T_s} \left(-\frac{R_s}{L_q} i_q - \frac{\omega_r \left(L_d i_d + \psi_f\right)}{L_q} + \frac{u_q}{L_q}\right) dt \\ \quad \approx \dfrac{T_s}{L_q}[u_q - (R_s i_d + \omega_r L_d i_d + \omega_r \psi_f)] \\ \quad = \dfrac{T_s}{L_q}\left(u_q - u_q^*\right). \end{cases} \tag{10}$$

Assuming that the output voltage of the inverter is exactly equal to the ideal voltage vector, the current will remain constant under steady state, but it is obviously impossible to achieve this because the inverter has only eight discrete states. The direction of the current ripple vector generated by a nonzero voltage vector in one control cycle is the same as the vector difference of the applied voltage vector and the ideal voltage vector, and the vector of the ripple current generated by the zero vector is in the opposite direction of the ideal voltage vector, that is,

$$\Delta I = \frac{T_s}{L_s}\left(\boldsymbol{v}_k - \boldsymbol{v}_s^*\right) \tag{11}$$

where $\boldsymbol{v}_s^*$ is the ideal voltage vector, and $\boldsymbol{v}_k$ is the actual voltage vector generated by the inverter. The magnitude of eight voltage vectors is

$$|v_k| = 2V_{\mathrm{dc}}/3, (k = 1, 2, \ldots, 6) = 0, \quad (k = 0, 7). \tag{12}$$

Therefore, when the ideal voltage vector is small, such as $\boldsymbol{v}_{s1}^*$ in Fig. 5, the ripple current generated by the nonzero vector is larger than that of the zero vector. When the ideal voltage vector is large, such as $\boldsymbol{v}_{s2}^*$ in Fig. 5, the ripple current generated by nonzero vector is smaller than that of the zero vector.

According to the analysis earlier, when the motor is operation at low speed or under light load, the ideal voltage vector amplitude is small, and the current ripple generated by nonzero vectors is greater than that of the zero vectors. To make the equivalent synthetic vector during a period of time roughly equal to the ideal voltage vector, more zero vector needs to be used. Conversely, when the motor speed is higher or the load is heavier, the ideal voltage vector magnitude is larger, and the ripple current produced by the nonzero vector is smaller than the zero vector. To make the equivalent voltage vector synthesized during a period of time roughly equal to the ideal voltage vector, the use of zero vector will be greatly reduced.

According to the above-mentioned analysis, zero vector is urgently needed under light load conditions. If the zero vector is forbidden, it will seriously affect the current quality, which we do not want to see. Therefore, we use the method shown in (8) to set the value of J_{lim}, where K represents the ratio of the acceptable ripple current to the current command amplitude. As the value of J_{lim} increases as the load increases, the suppression of CMV also increases. It should be pointed out that the heavy-duty operation is a more common condition in industry and transportation than the no-load operation.

TABLE II
PMSM PARAMETERS

Parameters	Values
Dc-link voltage (V)	750
Rated power (kW)	119
Rated speed (rpm)	975
Rated torque (Nm)	1100
Rated current (A)	169
Pole pairs	2
R_s (Ω)	0.0778
L_d (H)	0.005
L_q (H)	0.01
ψ_f (Wb)	1.35

V. EXPERIMENTAL RESULTS

The experimental platform is shown in Fig. 6. This platform has successfully supported the development of various types of rail vehicle traction systems in China. It has been fully validated for the simulation of actual vehicle traction systems. Table II shows the PMSM parameters and rated values.

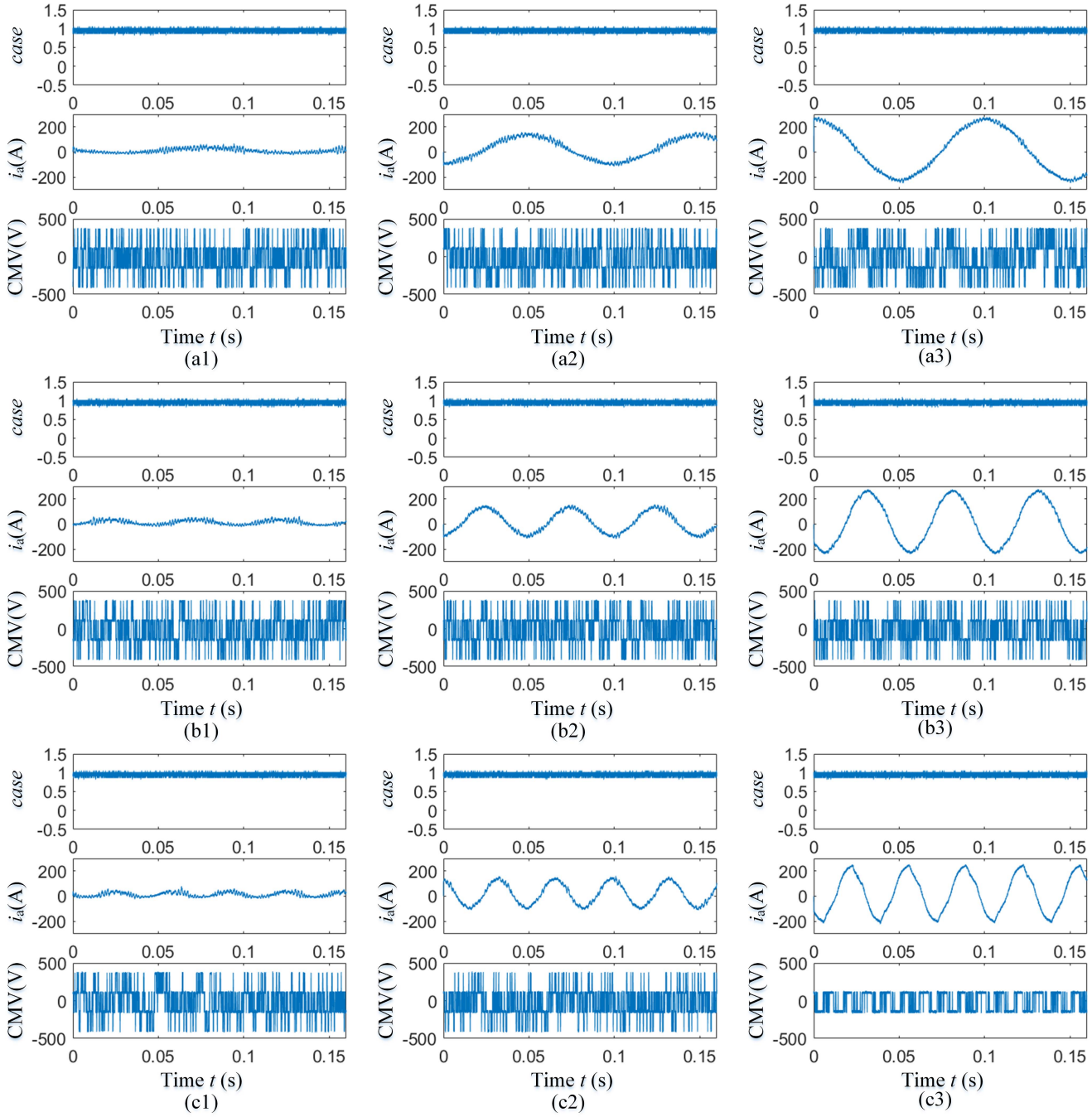

Fig. 8. Proposed method with $K = 0$ (equivalent with the conventional 4VVs method). (a1) 300 r/min, 10% load, and THD = 73.98%. (a2) 300 r/min, 50% load, and THD = 14.44%. (a3) 300 r/min, 100% load, and THD = 5.64%. (b1) 600 r/min, 10% load, and THD = 72.38%. (b2) 600 r/min, 50% load, and THD = 11.37%. (b3) 600 r/min, 100% load, and THD = 5.48%. (c1) 900 r/min, 10% load, and THD = 67.64%. (c2) 900 r/min,50% load, and THD = 12.13%. (c3) 900 r/min, 100% load, and THD = 7.57%.

The model of the motor and load runs in the dSPACE platform. The controller is a traction control unit (TCU) which was designed for metro vehicles. The TCU adopts 7U standard machinery and 19-in-wide standard chassis structure design. It adopts digital signal processor (DSP) + field-programmable gate array (FPGA) hardware control architecture. It has a wealth of peripherals including photoelectric conversion module, ADC module, digital I/O module, flash memory device, and communication module. The FCS-MPC algorithm is implemented by DSP (TMS320C6748). Sampling and driving pulses are performed by the FPGA. In this paper, the sampling interval T_s is set to be 100 μs. The host computer is used to download algorithm to the TCU, and the control desk is used to set the dSPACE. The sample and control data are stored and displayed by a HIOKI 8860-50 Memory Hicorder.

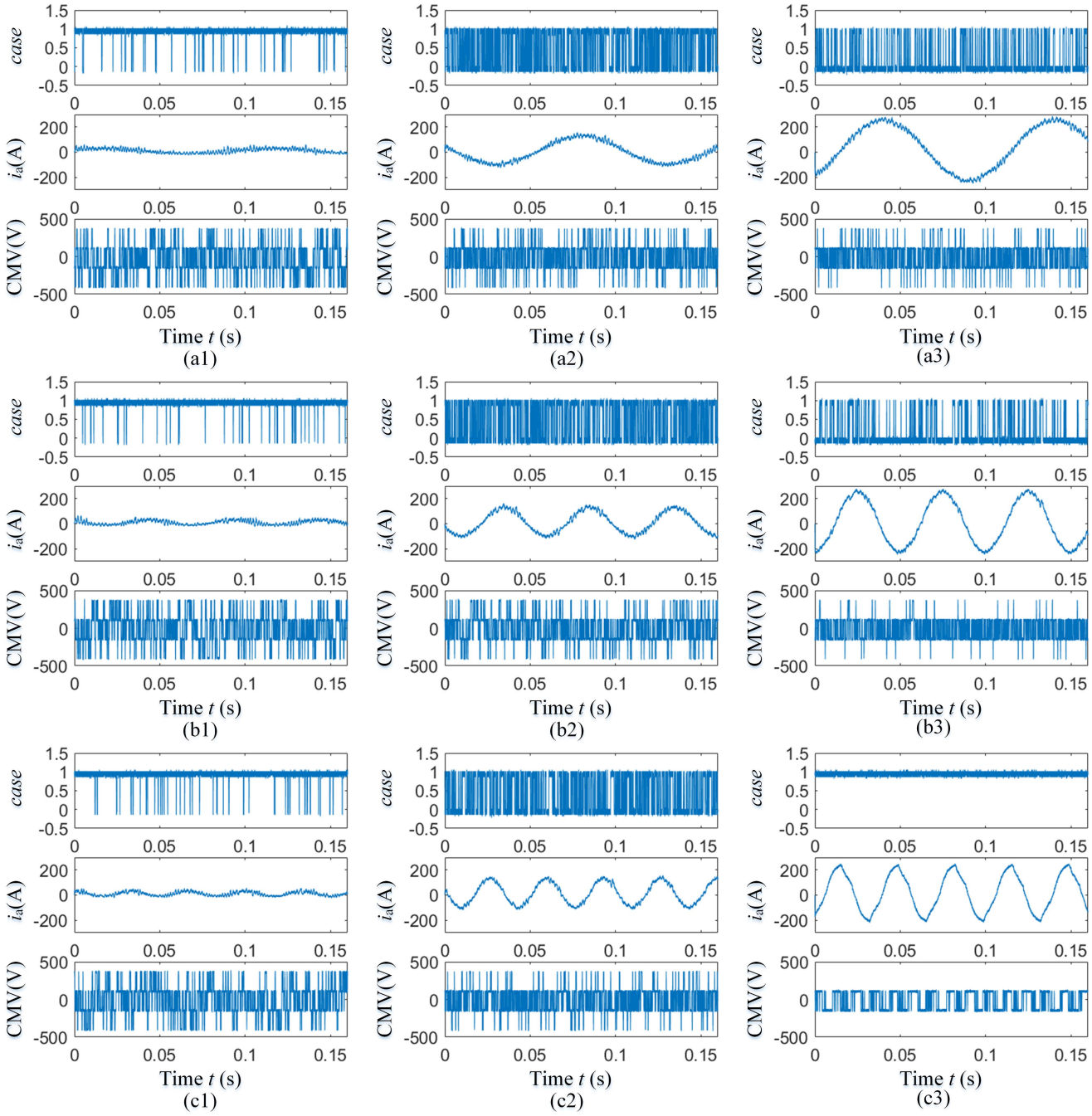

Fig. 9. Proposed method with $K = 0.05$. (a1) 300 r/min, 10% load, and THD = 76.77%. (a2) 300 r/min, 50% load, and THD = 14.01%. (a3) 300 r/min, 100% load, and THD = 7.09%. (b1) 600 r/min, 10% load, and THD = 67.55%. (b2) 600 r/min, 50% load, and THD = 14.63%. (b3) 600 r/min, 100% load, and THD = 6.13%. (c1) 900 r/min, 10% load, and THD = 63.46%. (c2) 900 r/min, 50% load, and THD = 12.32%. (c3) 900 r/min, 100% load, and THD = 7.71%.

For ease of comparison, several factors are used for evaluation. In order to quantitatively evaluate the suppression effect of CMV, the percentage of zero vector usage ZV% is defined as

$$\mathrm{ZV\%} = \frac{100 \cdot N_0}{f_s} \tag{13}$$

where $f_s = 1/T_s$ is the sampling frequency and N_0 is the number of zero vectors used per second. Generally, THD is used to evaluate the current distortion, but it is unfair to compare THD under different switching frequencies, so the product P of the two can be used as an important factor

$$P = \mathrm{THD\%} \cdot f_{\mathrm{seq}} = \mathrm{THD\%} \cdot \frac{N_s}{\Delta T} \tag{14}$$

where the equivalent switching frequency f_{seq} is calculated from the number of switching times N_s in a period of time ΔT (100 ms in this paper).

When the motor is operating at speed $n = 600$ r/min with 100% load, Fig. 7 shows the case flag (waveform on the top), phase current (waveform in the middle),

and CMV (waveform at the bottom) when K equal to 0, 0.04, and 0.08, respectively. Case flag case = 1 indicates that the zero vector has been abandoned, whereas case = 0 indicates that the zero vector is contained in the FCS. When $K = 0$ [see Fig. 7(a)], the proposed method is equivalent to the conventional 4VVs method, so case = 1 all the time. In this mode, the THD of i_a is 5.57% and zero vector which can lead to CMV $= \pm V_{\rm dc}/2$ is used very frequently. When $K = 0.04$ and 0.08 [see Fig. 7(b) and (c)], CMV is greatly suppressed because zero vector is abandoned when case = 0. In this mode, the THD of i_a is 6.21% and 6.56%, respectively, which shows that the current quality is slightly lower than that of the conventional 4VVs method but it is still within the acceptable range.

When $K = 0$, the proposed method is equivalent to the conventional 4VVs method. Fig. 8 shows the waveforms at different speeds and load conditions. It can be seen that there are more zero vector usages at low speed and light load conditions, and less frequent use of zero vectors at high speeds and heavy loads.

When $K = 0.05$, Fig. 9 shows the waveforms at different speeds and load conditions. Comparing Figs. 8 and 9, we can see that in order to ensure the current quality, the strength of CMV suppression varies according to speed and load conditions. Under light load conditions [see Figs. 8(a1)–(c1) and 9(a1)–(c1)], zero vectors are extremely needed to maintain the current quality, that is, the CMV suppression is weak. As for heavy load conditions [see Figs. 8(a3) and (b3) and 9(a3) and (b3)], the necessity of using zero vectors is weaker, so it is more easily to abandon them. As a special case [see Figs. 8(c3) and 9(c3)], the ideal voltage vector is close to the output limit of the inverter, so the zero vector is not used any more.

Fig. 10(a) shows the values of ZV% of the conventional 4VVs method and the nonzero 4VVs method. For the conventional 4VVs method, according to the analysis in Section IV-B, when the motor is operation at low speed or under light load, more zero vectors are used to maintain acceptable current ripple so that the percentage of zero vectors is up to 25.49. Conversely, when the motor speed is higher or the load is heavier, the use of zero vector is less. Nonzero 4VVs method does not use zero vectors so that ZV% equal to zero. In other words, nonzero 4VVs method shows very good performance on CMV suppression.

Fig. 10(b) shows the values of ZV% of the proposed method with different K. Compared to the two methods in Fig. 10(a), the proposed method exhibits a compromise performance in terms of CMV suppression, with the percentage of zero vectors lower than that of the conventional 4VVs method but higher than that of the nonzero 4VVs method. In addition, from the trend of ZV% versus stator current magnitude and the operation speed, it can be seen that the proposed method has stronger suppression effect on CMV under heavy load conditions than under light load. In fact, the heavy-duty operation is a more common condition in most industrial applications.

Fig. 11(a) shows the equivalent switching frequency $f_{\rm seq}$ of three different methods: conventional 4VVs method, nonzero

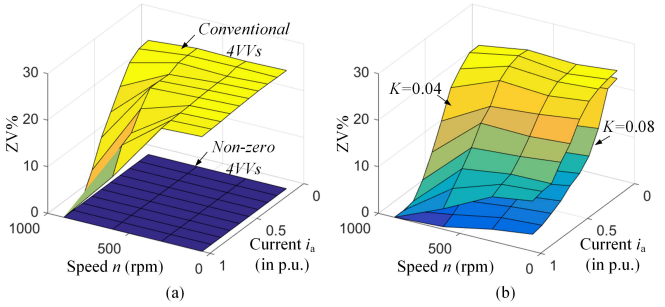

Fig. 10. Percentage of zero vectors usage ZV% versus stator current magnitude and the operation speed of PMSM. (a) Conventional and nonzero 4VVs methods. (b) Proposed method with $K = 0.04$ and $K = 0.08$.

TABLE III
COMPARISON OF DIFFERENT METHODS OPERATING FOR 100% LOAD

Speed	Methods	ZV%	THD%	f_{seq}	$P \cdot 10^{-3}$
50rpm	Conventional 4VVs	21.24	6.90	1114	7.69
	Non-zero 4VVs	0	7.07	1405	9.93
	Proposed method (K=0.04)	6.84	7.38	1013	7.48
	Proposed method (K=0.08)	1.68	7.71	1004	7.74
600rpm	Conventional 4VVs	10.25	5.48	1005	5.51
	Non-zero 4VVs	0	5.94	1241	7.37
	Proposed method (K=0.04)	3.79	5.83	959	5.59
	Proposed method (K=0.08)	0.41	6.31	912	5.75

4VVs method, and the proposed method. We can see that the switching frequency of the nonzero 4VVs method is about 1500 Hz, which is significantly higher than the other two methods. Since the proposed method does not use nonadjacent voltage vectors, the switching frequency is not significantly greater than the conventional 4VVs method, which is about 1000 Hz. Therefore, the proposed method is particularly suitable for applications where the switching frequency is strictly limited.

Fig. 11(b) and (c) shows a comparison of the current quality of the three methods. Fig. 11(b) is the current THD% versus stator current magnitude, while Fig. 11(c) is the product P of THD% and switching frequency $f_{\rm seq}$ versus stator current magnitude. Although the current THD of the three methods is almost the same, the conventional method does not have the effect of CMV suppression. Compared to nonzero 4VVs method, the proposed method can achieve almost the same current quality at the expense of a lower switching frequency.

Table III is a value-based table for comparing the CMV, current THD, and switching frequency when PMSM drive is operated for two different speeds at full load with

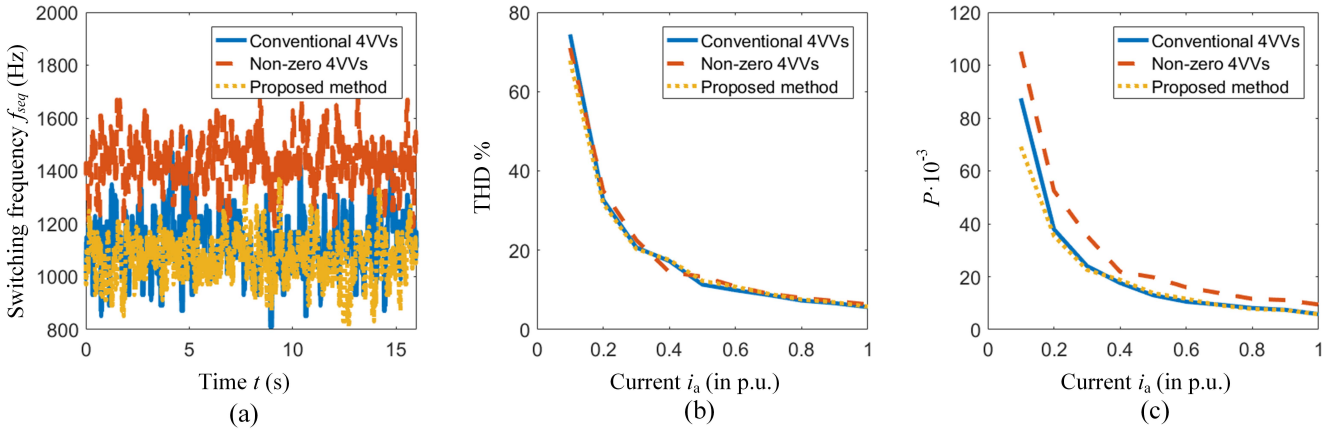

Fig. 11. Switching frequency and current quality comparison of three methods. (a) Equivalent switching frequency f_{seq}. versus time. (b) Current THD% versus current i_a. (c) Product of f_{seq} and THD% P versus current i_a.

different methods. In terms of CMV suppression, there is no doubt that the nonzero 4VVs method has won the top spot because ZV% is equal to zero. Comparing the proposed method with the conventional 4VVs method, when $K = 0.04$, ZV% decreased from 21.24 to 6.84 ($n = 50$ r/min) and from 10.25 to 3.79 ($n = 600$ r/min). When $K = 0.08$, this factor will be further reduced to 1.68 ($n = 50$ r/min) and 0.41 ($n = 600$ r/min). For the equivalent switching frequency f_{seq}, current THD%, and the product P of the two, the proposed method is comparable to the conventional 4VVs method. Due to the switching between nonadjacent voltage vectors, the values of f_{seq} and P of the nonzero 4VVs method are higher than that of the other two methods. The P value increased from 7.69 to 9.93 ($n = 50$ r/min) and from 5.51 to 7.37 ($n = 600$ r/min).

VI. Conclusion

Based on FCS-MPC, this paper presents a CMV suppression method considering the current ripple. A variable FCS is adapted based on a cost function limit related to current ripple. This method takes into account both CMV suppression and current quality maintenance without increasing the switching frequency.

By modeling the ripple current, the relationship between the probability of using zero vector and the operating conditions is analyzed. It is found that the zero vector needs to be used in a large amount under low speed and light load conditions, and the zero vector usage requirement is naturally reduced when the voltage is close to maximum value. Therefore, the proposed method focuses on reducing the probability of using zero vectors under heavy load conditions, which is the most common in industrial applications. The experimental results show that the zero vector percentage ZV% is reduced by 68% ($K = 0.04$) and 92% ($K = 0.08$) compared to the conventional 4VVs method at 50-r/min full load operation. At 600-r/min full load operation, ZV% is reduced by 63% ($K = 0.04$) and 96% ($K = 0.08$) compared to the conventional 4VVs method.

At the same sampling interval (100 μs in this paper), there is no significant difference in current THD between the three methods. Nonzero 4VVs method provides a good way to suppress CMV, but the equivalent switching frequency f_{seq} and P values are increased compared to the conventional 4VVs method. Since the proposed method uses only adjacent vectors like conventional 4VVs method, f_{seq}, and P values remain as low as the conventional 4VVs method. This is important in applications where switching frequency is critical. For example, rail transit traction systems generally require a switching frequency below 1000 Hz.

References

[1] H. Chen and H. Zhao, "Review on pulse-width modulation strategies for common-mode voltage reduction in three-phase voltage-source inverters," *IET Power Electron.*, vol. 9, no. 14, pp. 2611–2620, 2016.

[2] A. M. Hava and E. Ün, "A high-performance PWM algorithm for common-mode voltage reduction in three-phase voltage source inverters," *IEEE Trans. Power Electron.*, vol. 26, no. 7, pp. 1998–2008, Jul. 2011.

[3] R. M. Tallam, R. J. Kerkman, D. Leggate, and R. A. Lukaszewski, "Common-mode voltage reduction PWM algorithm for AC drives," *IEEE Trans. Ind. Appl.*, vol. 46, no. 5, pp. 1959–1969, Sep. 2010.

[4] Y.-S. Lai and F.-S. Shyu, "Optimal common-mode Voltage reduction PWM technique for inverter control with consideration of the dead-time effects—Part I: Basic development," *IEEE Trans. Ind. Appl.*, vol. 40, no. 6, pp. 1605–1612, Nov. 2004.

[5] N. Zhu, "Common-mode voltage mitigation by novel integrated chokes and modulation techniques in power converter systems," Ph.D. dissertation, Dept. Elect. Comput. Eng., Ryerson Univ., Toronto, ON, Canada, 2013.

[6] E. Un and A. M. Hava, "A near-state PWM method with reduced switching losses and reduced common-mode voltage for three-phase voltage source inverters," *IEEE Trans. Ind. Appl.*, vol. 45, no. 2, pp. 782–793, Mar. 2009.

[7] M. C. Cavalcanti, K. C. de Oliveira, A. M. de Farias, F. A. S. Neves, G. M. S. Azevedo, and F. C. Camboim, "Modulation techniques to eliminate leakage currents in transformerless three-phase photovoltaic systems," *IEEE Trans. Ind. Electron.*, vol. 57, no. 4, pp. 1360–1368, Apr. 2010.

[8] M. Cacciato, A. Consoli, G. Scarcella, and A. Testa, "Reduction of common-mode currents in PWM inverter motor drives," *IEEE Trans. Ind. Appl.*, vol. 35, no. 2, pp. 469–476, Mar. 1999.

[9] X. Guo, D. Xu, and B. Wu, "Common-mode voltage mitigation for back-to-back current-source converter with optimal space-vector modulation," *IEEE Trans. Power Electron.*, vol. 31, no. 1, pp. 688–697, Jan. 2016.

[10] V. Yaramasu, B. Wu, M. Rivera, M. Narimani, S. Kouro, and J. Rodriguez, "Generalised approach for predictive control with common-mode voltage mitigation in multilevel diode-clamped converters," *IET Power Electron.*, vol. 8, no. 8, pp. 1440–1450, 2015.

[11] S. K. Hoseini, J. Adabi, and A. Sheikholeslami, "Predictive modulation schemes to reduce common-mode voltage in three-phase inverters-fed AC drive systems," *IET Power Electron.*, vol. 7, no. 4, pp. 840–849, Apr. 2014.
[12] S. Mun and S. Kwak, "Reducing common-mode voltage of three-phase VSIs using the predictive current control method based on reference voltage," *J. Power Electron.*, vol. 15, no. 3, pp. 712–720, 2015.
[13] S. Kwak and S. K. Mun, "Model predictive control methods to reduce common-mode voltage for three-phase voltage source inverters," *IEEE Trans. Power Electron.*, vol. 30, no. 9, pp. 5019–5035, Sep. 2015.
[14] M. Preindl, E. Schaltz, and P. Thogersen, "Switching frequency reduction using model predictive direct current control for high-power voltage source inverters," *IEEE Trans. Ind. Electron.*, vol. 58, no. 7, pp. 2826–2835, Jul. 2011.
[15] L. Guo, X. Zhang, S. Yang, Z. Xie, and R. Cao, "A model predictive control-based common-mode voltage suppression strategy for voltage-source inverter," *IEEE Trans. Ind. Electron.*, vol. 63, no. 10, pp. 6115–6125, Oct. 2016.
[16] S. Vazquez, J. Rodriguez, M. Rivera, L. G. Franquelo, and M. Norambuena, "Model predictive control for power converters and drives: Advances and trends," *IEEE Trans. Ind. Electron.*, vol. 64, no. 2, pp. 935–947, Feb. 2017.
[17] Y. Zhang and H. Yang, "Two-vector-based model predictive torque control without weighting factors for induction motor drives," *IEEE Trans. Power Electron.*, vol. 31, no. 2, pp. 1381–1390, Feb. 2015.
[18] W. Xie *et al.*, "Finite-control-set model predictive torque control with a deadbeat solution for PMSM drives," *IEEE Trans. Ind. Electron.*, vol. 62, no. 9, pp. 5402–5410, Sep. 2015.
[19] J. Scoltock, T. Geyer, and U. K. Madawala, "A comparison of model predictive control schemes for MV induction motor drives," *IEEE Trans. Ind. Informat.*, vol. 9, no. 2, pp. 909–919, May 2013.
[20] W. Wang, J. Zhang, and M. Cheng, "Common model predictive control for permanent-magnet synchronous machine drives considering single-phase open-circuit fault," *IEEE Trans. Power Electron.*, vol. 32, no. 7, pp. 5862–5872, Jul. 2017.
[21] X. Zhang, B. Hou, and Y. Mei, "Deadbeat predictive current control of permanent-magnet synchronous motors with stator current and disturbance observer," *IEEE Trans. Power Electron.*, vol. 32, no. 5, pp. 3818–3834, May 2017.
[22] M. Siami, D. A. Khaburi, and J. Rodíguez, "Torque ripple reduction of predictive torque control for PMSM drives with parameter mismatch," *IEEE Trans. Power Electron.*, vol. 32, no. 9, pp. 7160–7168, Sep. 2017.
[23] M. Siami, D. A. Khaburi, and J. Rodriguez, "Simplified finite control set-model predictive control for matrix converter-fed PMSM drives," *IEEE Trans. Power. Electron.*, vol. 33, no. 3, pp. 2438–2446, Mar. 2018.
[24] M. Yang, X. Lang, J. Long, and D. Xu, "Flux immunity robust predictive current control with incremental model and extended state observer for PMSM drive," *IEEE Trans. Power Electron.*, vol. 32, no. 12, pp. 9267–9279, Dec. 2017.
[25] P. Kakosimos and H. Abu-Rub, "Predictive speed control with short prediction horizon for permanent magnet synchronous motor drives," *IEEE Trans. Power Electron.*, vol. 33, no. 3, pp. 2740–2750, Mar. 2018.
[26] Z. Zhou, C. Xia, Y. Yan, Z. Wang, and T. Shi, "Torque ripple minimization of predictive torque control for PMSM with extended control set," *IEEE Trans. Ind. Electron.*, vol. 64, no. 9, pp. 6930–6939, Sep. 2017.
[27] X. Zhang and B. Hou, "Double vectors model predictive torque control without weighting factor based on voltage tracking error," *IEEE Trans. Power Electron.*, vol. 33, no. 3, pp. 2368–2380, Mar. 2018.
[28] Z. Zhang, Z. Li, M. P. Kazmierkowski, J. Rodríguez, and R. Kennel, "Robust predictive control of three-level NPC back-to-back power converter PMSG wind turbine systems with revised predictions," *IEEE Trans. Power Electron.*, vol. 33, no. 11, pp. 9588–9598, Nov. 2018.
[29] L. Wang *et al.*, "A finite control set model predictive control method for matrix converter with zero common-mode voltage," *IEEE J. Emerg. Sel. Topics Power Electron.*, vol. 6, no. 1, pp. 327–338, Mar. 2018.
[30] M. Norambuena, P. Lezana, and J. Rodriguez, "A method to eliminate steady state error of model predictive control in power electronics," *IEEE J. Emerg. Sel. Topic Power Elect.*, to be published. doi: 10.1109/JESTPE.2019.2894993.
[31] Z. Chen, J. Qiu, and M. Jin, "Prediction-error-driven position estimation method for finite control set model predictive control of interior permanent magnet synchronous motors," *IEEE J. Emerg. Sel. Topic Power Elect.*, to be published. doi: 10.1109/JESTPE.2018.2870905.
[32] J. J. Aciego, I. Gonzalez-Prieto, and M. J. Duran, "Model predictive control of six-phase induction motor drives using virtual voltage vectors," *IEEE J. Emerg. Sel. Topic Power Elect.*, vol. 65, no. 1, pp. 27–37, Jan. 2018.

Xiaofan Wang (S'16) received the B.S. degree in electrical engineering from Beijing Jiaotong University, Beijing, China, in 2014, where he is currently pursuing the Ph.D. degree with the School of Electrical Engineering.

His current research interests include traction converters and motor drives and digital control of power electronic-based devices.

Xiaochun Fang (S'14–M'17) received the B.S. and Ph.D. degrees in engineering from Beijing Jiaotong University, Beijing, China, in 2010 and 2016, respectively.

He is currently a Lecturer with the School of Electrical Engineering, Beijing Jiaotong University. His current research interests include traction converters and motor drives, energy management for railway systems, IGBT fault mechanisms, and failure prediction.

Shuai Lin received the B.S. degree in electrical engineering from Beijing Jiaotong University, Beijing, China, in 2017, where he is currently pursuing the Ph.D. degree with the School of Electrical Engineering.

His current research interests include motor drives and reliability of traction drive systems.

Fei Lin (M'05) received the B.S. degree in electrical engineering from Xi'an Jiaotong University, Xi'an, China, in 1997, the M.S. degree in electrical engineering from Shandong University, Jinan, China, in 2000, and the Ph.D. degree in electrical engineering from Tsinghua University, Beijing, China, in 2004.

He is currently a Professor with the School of Electrical Engineering, Beijing Jiaotong University, Beijing. His current research interests include traction converters and motor drives, energy management for railway systems, and digital control of power electronic-based devices.

Zhongping Yang (M'14) received the B.Eng. degree in electrical engineering from the Tokyo University of Mercantile Marine, Tokyo, Japan, in 1997, and the M.Eng. and Ph.D. degrees in electrical engineering from the University of Tokyo, Tokyo, in 1999 and 2002, respectively,.

He is currently a Professor with the School of Electrical Engineering, Beijing Jiaotong University, Beijing, China. His current research interests include high-speed rail integration technology, traction and regenerative braking technology, and wireless power transfer of urban rail vehicles.

Dr. Yang was a recipient of the Zhan Tianyou Award for Science and Technology in 2010, the Excellent Popular Science and Technology Book Award in 2011, and the Science and Technology Progress Award (Second Prize) of Ministry of Education in China in 2016.